A facile preparation of nitrogen-doped porous carbons from renewable as efficient catalysts for oxygen reduction reaction

Junhong Ma, Minhui Shi, Tuan K.A. Hoang, Zhizi Yao, Akang Sun

PII: S0022-4596(20)30439-4

DOI: https://doi.org/10.1016/j.jssc.2020.121609

Reference: YJSSC 121609

To appear in: *Journal of Solid State Chemistry*

Received Date: 16 June 2020

Revised Date: 20 July 2020

Accepted Date: 23 July 2020

Please cite this article as: J. Ma, M. Shi, T.K.A. Hoang, Z. Yao, A. Sun, A facile preparation of nitrogen-doped porous carbons from renewable as efficient catalysts for oxygen reduction reaction, *Journal of Solid State Chemistry* (2020), doi: https://doi.org/10.1016/j.jssc.2020.121609.

Junhong Ma: Conceptualization, Methodology, Supervision.

Minhui Shi: Investigation, Writing-Original draft preparation.

Tuan K.A. Hoang: Writing- Reviewing and Editing.

Zhizi Yao: Data curation.

Akang Sun*:* Validation.

A facile preparation of nitrogen-doped porous carbons from renewable as efficient catalysts for oxygen reduction reaction

Junhong Ma [1,2,*], Minhui Shi [1,2] , Tuan K.A. Hoang [3], Zhizi Yao [1] & Akang Sun [1]

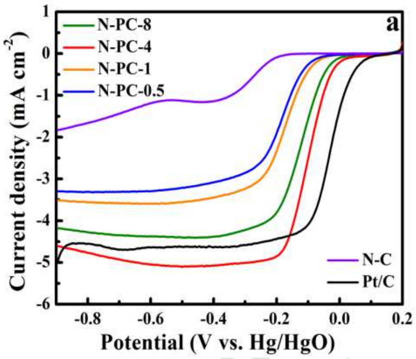

A facile preparation of nitrogen-doped porous carbons from renewable as efficient catalysts for oxygen reduction reaction

Junhong Ma [1,2,*], Minhui Shi [1,2] , Tuan K.A. Hoang [3], Zhizi Yao [1] & Akang Sun [1]

[1] *College of Chemistry and Chemical Engineering, Xinjiang University, Urumqi 830046, Xinjiang P. R. China*

[2] *Key Laboratory of Energy Materials Chemistry, Ministry of Education; Institute of Applied Chemistry, Xinjiang University, Urumqi, 830046, Xinjiang P. R. China*

[3] *Department of Chemical Engineering and Waterloo Institute of Nanotechnology, University of Waterloo, Waterloo, Ontario, N2L3G1, Canada*

[*] *To whom correspondence should be addressed. E−mail: majhxju@163.com*

Abstract

Developing cost-effective and high active catalysts for the oxygen reduction reaction (ORR) is vital for the application of fuel cells. In this work, nitrogen-doped porous carbon nanosheets(N-PC) derived from biomass waste soybean residue were prepared by a facile combining method of solid state grinding and pyrolysing, using g-C_3N_4 as both nitrogen source and sacrificial template. The benefit of this facile process is that neither a designated template nor a chemical activating agent is required. The influence of g-C_3N_4 level on the structure and ORR behavior of the resulting N-PC was systematically investigated by means of spectroscopy (XPS), surface area analysis (BET), electron microscopy (TEM, SEM) et al., and electrochemical experiments. The optimized sample possesses appropriate defect structure, high BET surface area and pore volume (483 m^2 g^{-1} and 1.57 cm^3 g^{-1}), and high N content (6.04 at.%), and exhibits decent activity and methanol tolerance in ORR process. Its superior stability versus the commercial Pt/C is also evidenced by almost 50 % higher in chronoamperometric current response after 3600 seconds testing duration. This work supplies a simple and economical route to synthesize superior electrocatalyst for ORR on the basis of biomass waste.

Keywords: Biomass waste; Nitrogen doped carbon; Oxygen reduction reaction; Fuel cell.

1 . Introduction

Fuel cells are an alternative, more efficient, green energy source and represent a focus of many researchers. In fuel cells, the cathode oxygen reduction reaction (ORR) is an essential step, but it is currently suffering from sluggish kinetics [1-4]. Pt-based catalysts are often applied in ORR due to excellent electrochemical activity [5,6], but the exorbitant price, limited stability, and poor resistance to CH_3OH impede the application of Pt-based catalysts in ORR [7,8]. Thus, researchers started to develop some economical and efficient catalysts as a substitution for Pt. Among these catalysts, nitrogen-doped carbon materials (N-C) present excellent electrocatalytic performance in ORR thanks to their unique electronic properties [9].

Recently, exploiting biomass resources to build catalysts has drawn increased attention of researchers, owing to its low-cost and recyclability. The unique properties and high content of C and N elements endow the biomass with a potential to prepare porous N-C materials for electrocatalysis [10-13]. Zhang and his co-workers synthesized N-C mesoporous materials containing a considerable pyridinic-N content of 11.58 at.% from chitosan. The obtained N-C possessed a huge surface area (SA) of 1190 m^2 g^{-1}, and exhibited excellent ORR activity in alkaline solution [10]. Liu et al. fabricated a graphene-like porous N-C material from fruits of glossy privet. The prepared catalyst had high specific surface areas, good conductivity, a certain number of doped N atoms, topological defects, and presented remarkable ORR activity [12]. Unfortunately, the proposed methods were complicated.

Additionally, adopting the appropriate method to generate and adjust the pore structure of N-C materials is of great importance, since the property of porous structure in carbon materials is directly related to the specific surface area, defect degree, electron/ion transfer, and N doping, and thus the ORR performance. Now, the general strategy to synthesize porous N-C catalysts is using a template or activation agent [14-17]. For instance, Cao et al. used ZIF-7 as template and glucose as carbon feedstock to produce N-doped porous carbon [17], which exhibits excellent electrocatalytic activity for ORR. Subashchandrabose’s group fabricated hierarchical N-C with excellent electrocatalytic activity toward ORR, by using Borassus Flabellifer combined with a metal hydroxide activating agent [15]. However, for the template route, the cost was higher and more reaction steps were required to synthesize the template, use it, and remove it. Another method was to use activation agents, in which the harsh chemicals were often used as activating agents, and post-treatment of washing was also indispensable. In recent years, graphitic carbon nitride (g-C_3N_4) has been regarded as a superior material to synthesize N-doped porous carbon materials, since g-C_3N_4 contains a lot of N (57.1 at.%), and has easily tailorable structure. These characteristics indicate that g-C_3N_4 can be applied both as template and N source for preparing porous N-C. Additionally, g-C_3N_4 could completely decompose at the temperatures above 710 ℃ [18]. Thus, extra template removing operation could be omitted during the N-C material preparation. For instance, Zhang et al. acquired N-C nanosheets with micro- and mesopores via carbonizing glucose coated with g-C_3N_4, the optimal catalyst possessed high percentage of N (11.6 at.%) and SA (1077 m^2 g^{-1}), and showing improved ORR activity, stability, and methanol resistance with respect to commercial Pt/C catalyst [19]. Li and his co-workers fabricated chitin and g-C_3N_4 composites derived N-doped carbon via the low-temperature dissolution and carbonization, the obtained product displayed excellent activity toward ORR [20].

Here, we provide a very simple procedure for preparing N-doped hierarchical porous carbon nanosheets (N-PC), using the waste soybean residue as the C source, and g-C_3N_4 as both nitrogen source and sacrificial template. The effect of g-C_3N_4 dosage on the composition and structure of the obtained N-PC was comprehensively investigated. Though previous research works have demonstrated the possibility of using g-C_3N_4 for the preparation of N-doped porous carbon materials. To our knowledge, the systematic research of the synergy of N-doping and structure tuning determined by the g-C_3N_4 precursor level has not been reported. We demonstrate here that the optimal N-PC catalyst prepared with appropriate g-C_3N_4 amount presented decent ORR activity that can stand comparison with Pt/C, and its stability and CH_3OH tolerance are superior to Pt/C in ORR process.

2 . Experiments

2.1. Synthesis

All chemicals (analytical grade) were supplied from the commercial sources. The g-C_3N_4 was synthesized by pyrolysis of urea in static air, following the literature [21]. The purified soybean dregs (SDs) were obtained according to the procedure in the previous work [22].

0.25 g of SDs, a certain amount of g-C_3N_4, and 5 mL ethanol were firstly mixed thoroughly by grinding in an agate mortar, followed by annealing in a tube oven at 800 ℃ for 2 hours under nitrogen gas atmosphere, with a heating rate of 5 ℃ min^{-1}. The resulted materials are marked as N-PC-x, with x denotes mass ratio of g-C_3N_4 to SDs. To spotlight the role of g-C_3N_4, the reference sample N-C was prepared by an identical process without the addition of g-C_3N_4.

2.2. Physical and chemical characterizations

The surface morphology and structure of the catalyst samples were characterized by scanning electron microscope (SEM, Hitachi SU8010, Japan). Transmission electron microscopy (TEM) and selected area mapping were operated on a JEM-2100F instrument with acceleration voltage of 100 kV. The chemical composition of the catalyst's surface was studied by X-ray photoelectron spectroscopy (XPS) using ESCALAB 250 (Thermo Fisher Scientific, USA). Elemental analysis of C, N, and O were performed on an Elementar vario EL cube Elemental Analyzer. The Raman spectra were recorded upon irradiation at 532 nm using the Brüker Senterra R200-L microscope. Nitrogen adsorption and desorption were recorded on the nitrogen sorption apparatus (3H-2000PM1/2, China). The Barrett–Joyner–Halenda (BJH) model was used to analyze the obtained isotherms to deliver the specific SA, pore size distribution, and pore volume.

2.3. Electrochemical measurements

The ORR performance was measured on a WaveDriver 20 potentiostat/galvanostat station (PINE Research Instrumentation) using the standard, three-electrode system. The Hg/HgO electrode and platinum wire were used as the reference and the counter electrodes, respectively. The rotating ring-disk electrode (RRDE) or the rotating disk electrode (RDE) coated with the catalyst was utilized as a working electrode. The 5 mg catalyst was dispersed in 450 μL of isopropanol and 50 μL of Nafion (5 %). 5 μL of prepared dispersion was dropped accurately onto the RDE or RRDE electrode to fabricate the working electrode. Linear sweep voltammetry (LSV) was tested using oxygen saturated 0.1 M KOH at the scan rate of 5 mV s^{-1} between - 0.90 to 0.20 V. From the LSV curves recorded at rotation speeds from 400 to 2025 rpm, the number of transferred electrons (n) was calculated using the Koutecky-Levich (K-L) equation [23]:

$$1/J = 1/J_K + B^{-1}\omega^{-1/2} \qquad (1)$$

$$B = 0.2nF(D_o)^{2/3}\upsilon^{-1/6}C_o \qquad (2)$$

Tafel plots were derived from LSV profiles measured on RDE, and chronoamperometry (CA) was measured at the applied potential of - 0.30 V with 1600 rpm rotating speed. RRDE measurement was used to further provide the information of H_2O_2 yield by the followed equation:

$$n = 4 \times \frac{I_D}{I_D + \frac{I_R}{N}} \qquad (3)$$

$$H_2O_2\% = 200 \times \frac{I_R}{I_D \times N + I_R} \qquad (4)$$

Where I_D and I_R are measurement currents on disk and ring electrodes, respectively, N is the collection efficiency of ring electrode (37%). All potentials mentioned in this study are versus the potential of the standard Hg/HgO electrode.

3. Results and discussion

3.1. Physicochemical characterization analysis

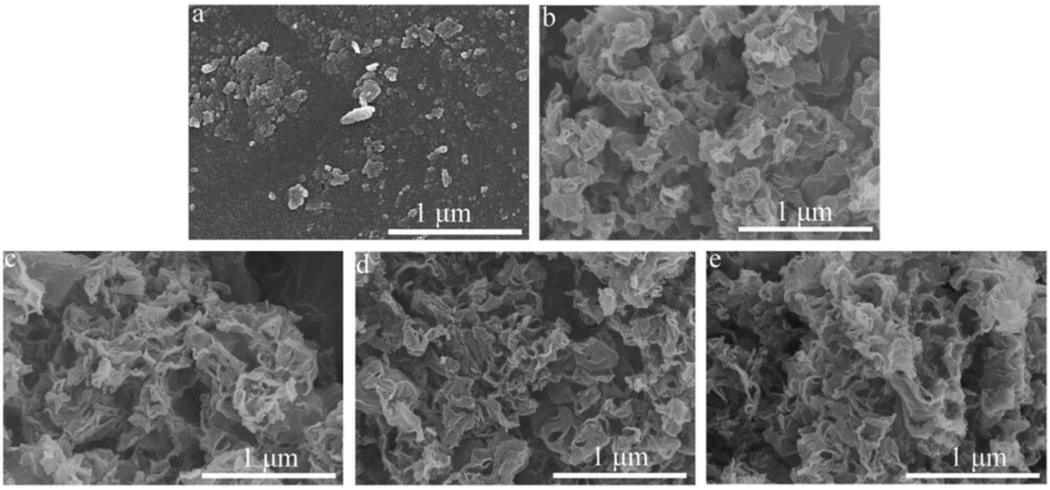

Fig. 1. SEM images of (a) N-C, (b) N-PC-0.5, (c) N-PC-1, (d) N-PC-4, and (e) N-PC-8.

Fig. 1 illustrates the SEM results of all as-prepared samples. N-C prepared without adding g-C_3N_4 exists in a compact and lumpy state with some small protuberances on its surface. Whilst the series of N-PC catalysts exhibit loose and curved nanosheets, and with the increase of g-C_3N_4 precursor amount from N-PC-0.5 to N-PC-8 the material structure is more fluffy and porous, which might be induced by the more gases were released during the pyrolysis process of g-C_3N_4. The crumpled and porous nanosheet structure in N-PC catalysts would be expected to provide high BET surface and pore volume, and may act favorably to the ORR process.

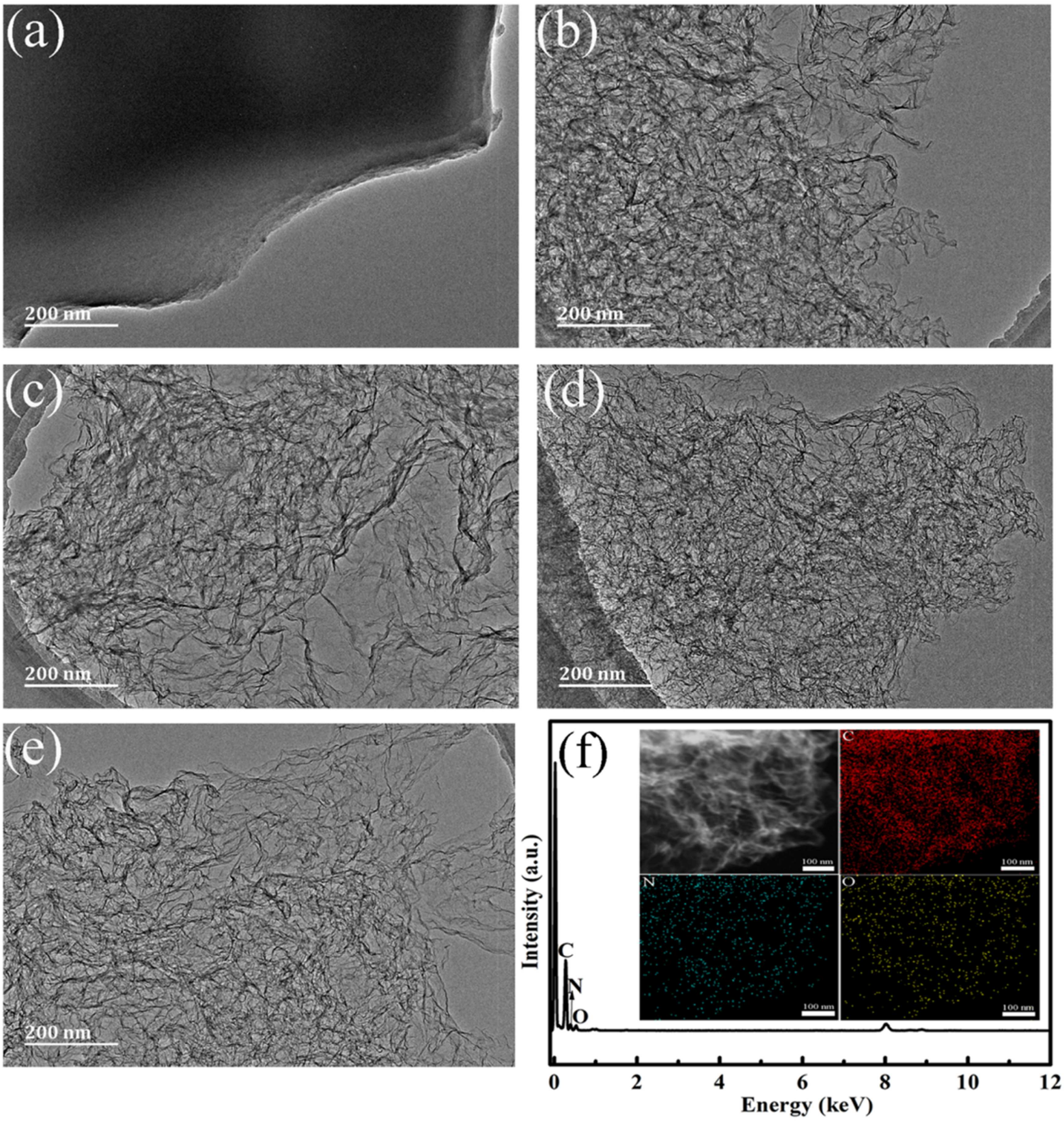

Fig. 2. TEM images of (a) N-C, (b) N-PC-0.5, (c) N-PC-1, (d) N-PC-4, (e) N-PC-8, and (f) EDS and elemental mapping images of N-PC-4.

The TEM were further characterized to present the morphology of all as-prepared samples. We can see that the N-C derived from pure soybean dregs exhibits dense structure without obvious pores. However, when g-C_3N_4 was introduced into the synthetic system, the obtained N-PC series samples possess wrinkled graphene-like structure with irregular pores (Fig. 2b-e), which would be conducted to the increase of surface area, active site exposure, and mass transfer. Fig. 2f shows the EDS and elemental mapping pattern of the typical N-PC-4 catalyst, It is apparent that N is well-dispersed throughout the sample, and this will help generate more N-C active sites.

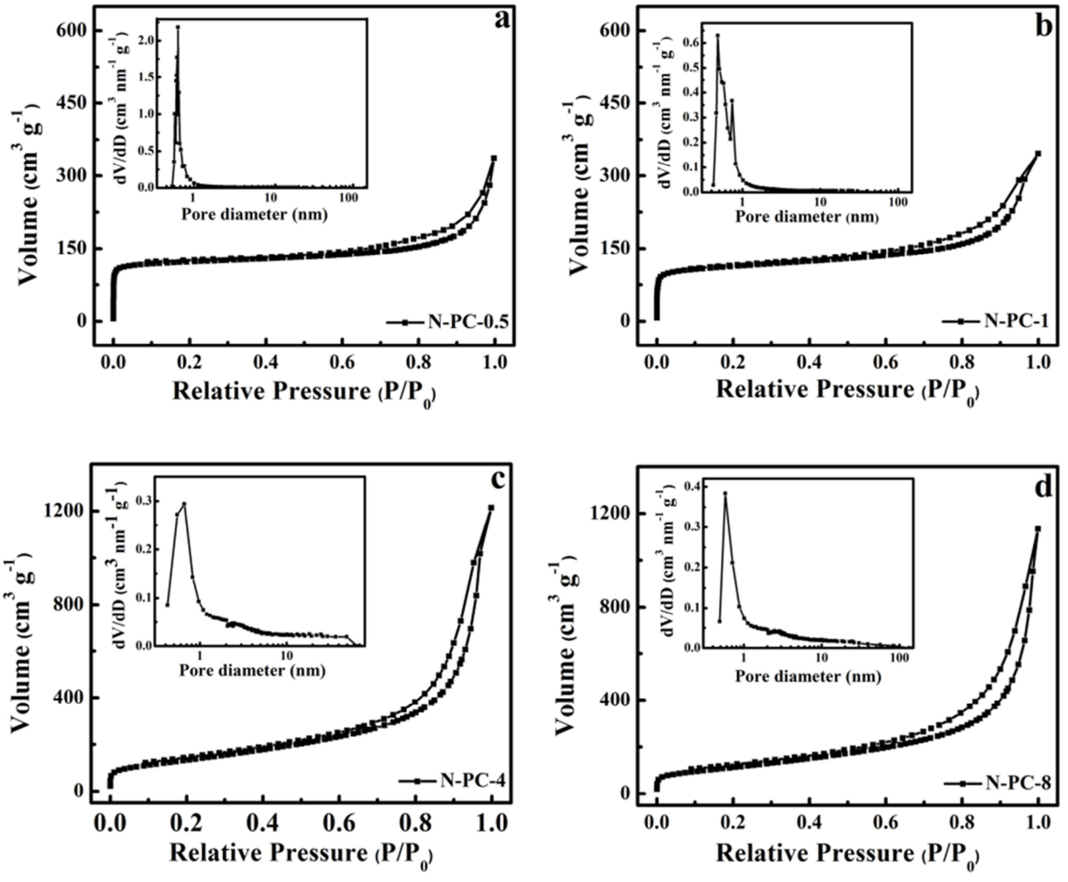

Fig. 3. N_2 adsorption-desorption isotherms and pore size distributions of (a) N-PC-0.5, (b) N-PC-1, (c) N-PC-4, and (d) N-PC-8.

N_2 adsorption/desorption was applied to estimate the SA and porosity of N-PC structures. As shown in Fig. 3, all N-PC catalysts present typical type IV isotherms. A vertical increase in the low relative pressure (p_r) region and an apparent hysteresis loop in the vicinity of high p_r means that micropores and mesopores coexist in the catalysts. A sharp peak centered around 0.6 nm can be clearly observed in the insets of Fig. 3, which is attributed to the microporous structure in N-PC samples. Moreover, it is obviously that with the increase of g-C_3N_4 precursor amount, the pore size distribution gradually widen from N-PC-0.5 to N-PC-8, the proportion of mesopore gradually increases and macropores begin to appear..

Table 1 Textural parameters of various samples

Sample	S_{BET}[a] (m^2 g^{-1})	V_T[b] (cm^3 g^{-1})	V_{micro}[c] (cm^3 g^{-1})	V_{meso}[d] (cm^3 g^{-1})	D_{ap}[e] (nm)
N-PC-0.5	478	0.43	0.19	0.24	4.36
N-PC-1	425	0.45	0.17	0.28	5.04
N-PC-4	483	1.57	0.20	1.37	15.53
N-PC-8	411	1.47	0.17	1.30	17.12

[a] Specific surface area. [b] Total pore volume. [c] Micropore volume. [d] Mesopore volume. [e] Average pore diameter.

From the textural parameters of N-PC samples (Table 1), we can see that, the micropore volumes of all N-PC are approximately 0.18 cm^3 g^{-1}, while the volume of mesopore is increased from 0.24 cm^3 g^{-1} of N-PC-0.5 to 1.37 cm^3 g^{-1} of N-PC-4, as well as the total volume from 0.43 cm^3 g^{-1} to 1.57 cm^3 g^{-1} , versus the increase of the g-C_3N_4 amount, except for the N-PC-8 in which the mesopore and total volumes go down to 1.30 cm^3 g^{-1} and 1.47 cm^3 g^{-1} , respectively. These results indicate that the g-C_3N_4 dosage has evident effect on the generation of mesopore structure. When the g-C_3N_4 precursor is added within a certain amount (from N-PC-0.5 to N-PC-4), the mesopore volume of the obtained N-PC materials significantly increases with the decomposition of g-C_3N_4. However, when the g-C_3N_4 level is excessive, a mass of gas released from g-C_3N_4 pyrolysis may cause the collapse of some mesopores to form macropores in

N-PC-8. It is worth noting that N-PC-4 shows biggest total and mesopore volumes (1.57 m^3 g^{-1} and 1.37 m^3 g^{-1}, respectively) in as-prepared N-PC samples, even though they all have the similar BET areas of around 450 m^2 g^{-1}.

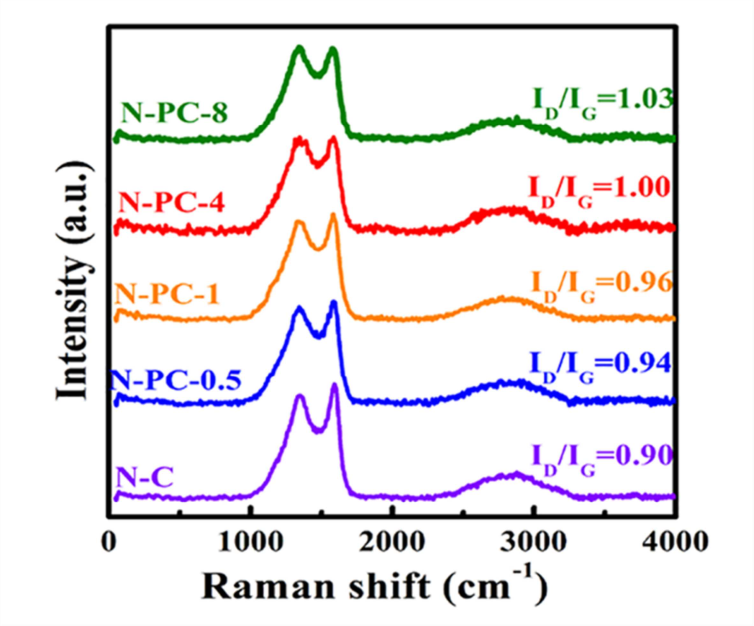

Fig. 4. Raman spectra of N-C, N-PC-0.5, N-PC-1, N-PC-4, and N-PC-8.

Raman spectroscopy was examined to research the graphitic degree and characterize the defect structures of all synthetic catalysts. As plotted in Fig. 4, all the as-prepared samples present distinct 2D bands at ca. 2700 cm^{-1} in Raman, indicating the formation of graphene-like layers in the N-C and N-PC [12]. Besides, two prominent peaks corresponding to the G band (1580 cm^{-1}) and D band (1350 cm^{-1}) are observed. The D band is related to the structural defect and disordering of graphitic C, and the G band is related to well-structured graphite. The relative intensity of two bands (I_D/I_G) is a descriptor of the structural defects of carbonaceous materials. The intensity ratios (I_D/I_G) of N-PC materials increase with the proportion of g-C_3N_4 in precursor mixture, from 0.94 of N-PC-0.5 to 1.03 of N-PC-8 (as shown in Fig. 4), signifying that the introduction of g-C_3N_4 is closely linked with the defect structure of the resulting N-PC samples. As we know, the appropriate defect structure in carbon-based catalysts would benefit to supply more active sites for ORR [24, 25].

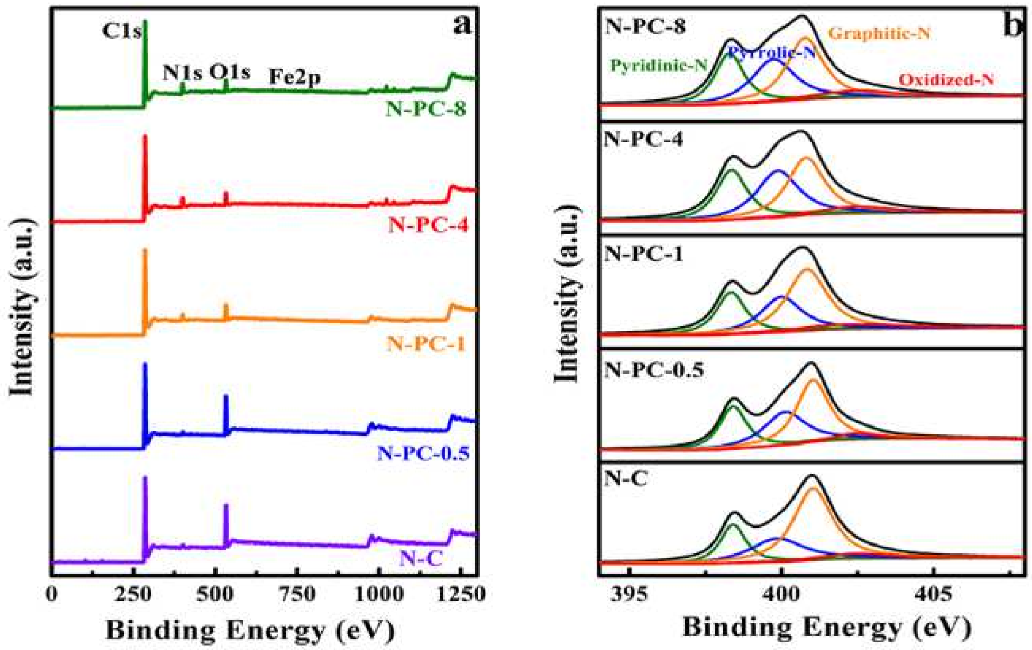

Fig. 5. (a) XPS surveys and (b) N 1s XPS spectra for N-C, N-PC-0.5, N-PC-1, N-PC-4, and N-PC-8.

The element composition and chemical state on the surface of all samples were analyzed using XPS (Fig. 5). The chemical compositions are summarized in Table 2. The XPS survey spectra show the co-existence of C, N, and O atoms in all samples (Fig. 5a). When increasing the quantity of the g-C_3N_4 precursor in the synthesis mixture, the nitrogen level increases from 2.05 at. % of N-C to 6.78 at. % of N-PC-8. This result reveals that much of surface N species in N-PC is originated from the g-C_3N_4. The N in carbon matrix can be associated with the pyridine N (398.4 eV), pyrrole N (399.9 eV), graphite N (401.0 eV), and oxidized N (402.5 eV) (Fig. 5b). In all synthesized materials, the sum of pyridinic N and the graphitic N is dominant, which is expected to be beneficial for ORR since both are generally considered as the active sites of carbon-based catalysts for ORR [13]. It is worth noting that the C contents of N-PC series samples also varies with the additive amount of g-C_3N_4. This might be due to that some of carbonaceous species derived from the g-C_3N_4 remain in the as-prepared N-PC materials [20, 22], and their levels are affected by nitrogen doping.

Table 2 Chemical composition obtained from XPS analysis for all samples

Sample	Composition (at.%)			N 1s (%)			
	C	N	O	pyridinic N	pyrrolic N	graphitic N	oxidized N
N-C	82.00	2.05	15.95	18.49	23.27	52.36	5.88
N-PC-0.5	83.18	2.07	14.75	24.20	28.69	42.55	4.56
N-PC-1	89.40	4.21	6.39	21.83	25.58	43.91	8.68
N-PC-4	85.62	6.04	8.34	25.54	31.92	35.46	7.08
N-PC-8	85.20	6.78	7.93	24.61	30.38	36.95	8.36

Table 3 shows the elementary analysis (EA) results of all as-prepared samples. It is apparent that the bulk N and C content also varies with the g-C_3N_4 amount, showing the similar variation trend as the XPS results. The bulk N amount increase from 6.77 wt. % of N-C to 11.17 wt. % of N-PC-8, according to their EA results.

Table 3 The content of C, N, and O obtained from elemental analysis

Sample	C (wt.%)	N (wt.%)	O (wt. %)
N-C	77.38	6.77	13.97
N-PC-0.5	79.13	7.75	11.64
N-PC-1	80.64	7.85	10.12
N-PC-4	77.20	9.30	11.84
N-PC-8	78.72	11.17	8.42

From the above discussion results, we can know that apart from being a nitrogen source, g-C_3N_4 is also act as a structure regulator. A moderate amount of g-C_3N_4 precursor can give rise to a porous graphene-like N-PC catalyst with high surface area and plenty mesopore on the basis of providing abundant N-C active sites, which would be expected to reach a superior synergy and boosting the ORR process. And that is why we did not use excessive g-C_3N_4 to further obtain N-PC with higher N content that might be comparable to those reported in the literature [26, 27].

3.2. Electrochemical performance in oxygen reduction reaction

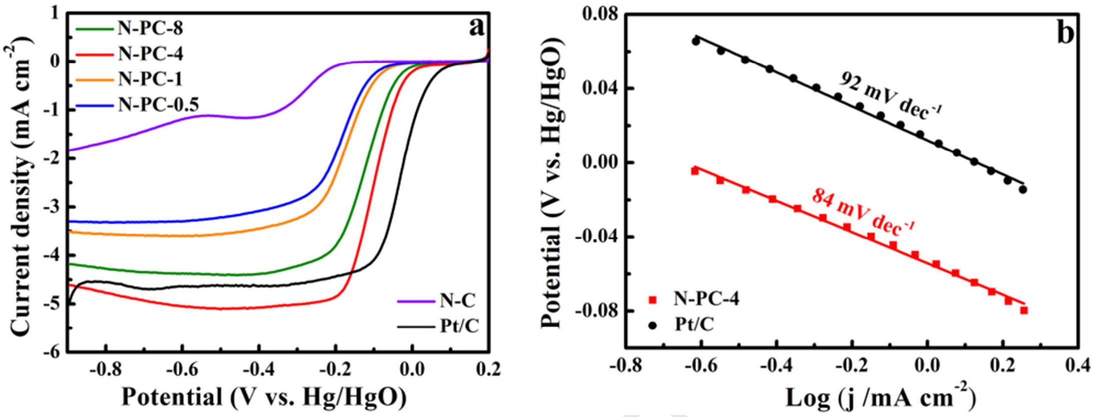

Fig. 6. (a) ORR polarization curves of all prepared samples and Pt/C in O_2 statured 0.1 M KOH with sweep rate of 5 mV s^{-1} at 1600 rpm. (b) Tafel plots of N-PC-4 sample and Pt/C catalysts.

Fig. 6a represents the LSV profiles of all as-prepared samples and Pt/C. The reference N-C sample shows the poorest ORR activity. When the mass ratios of g-C_3N_4 to SDs progressively increase from 0.5 to 4, the ORR activity of corresponding N-PC catalysts continues to rise. N-PC-4 shows best ORR activity as indicated by the most positive onset potential (E_{on}) of 0.03 V and half-wave potential ($E_{1/2}$) of - 0.10 V, which are only slightly negatively shifted vs. those of the Pt/C (E_{on} and $E_{1/2}$ are 0.09 V and -0.03 V, respectively). Moreover, N-PC-4 exhibits a larger limited current density (5.09 mA cm^{-2}) than commercial Pt/C (4.63 mA cm^{-2}). When further increasing the g-C_3N_4 amount, the ORR activity of the corresponding N-PC-8 drops to lower than that of the N-PC-4. The decent ORR activity of the N-PC-4 might be originated from the appropriate defect level, high BET SA and pore volume, and high N containing active sites, as discussed previously in the physical characterization sections (Raman, BET, and XPS analysis results). It should be noted that though the N-PC-8 possesses higher

N amount than N-PC-4, the relative poor electrical conductivity caused by the high defect degree, smaller surface area and pore volume (especially mesopore volume) might be the main reason for the low activity of N-PC-8 in comparison to N-PC-4. The Tafel plots of N-PC-4 and the Pt/C are presented and compared in Fig. 6b. At high potentials, the obtained slope of Tafel plot for N-PC-4 (84 mV dec^{-1}) is lower than the value for commercial Pt/C (92 mV dec^{-1}), suggesting that the former has faster electrocatalytic reaction kinetics.

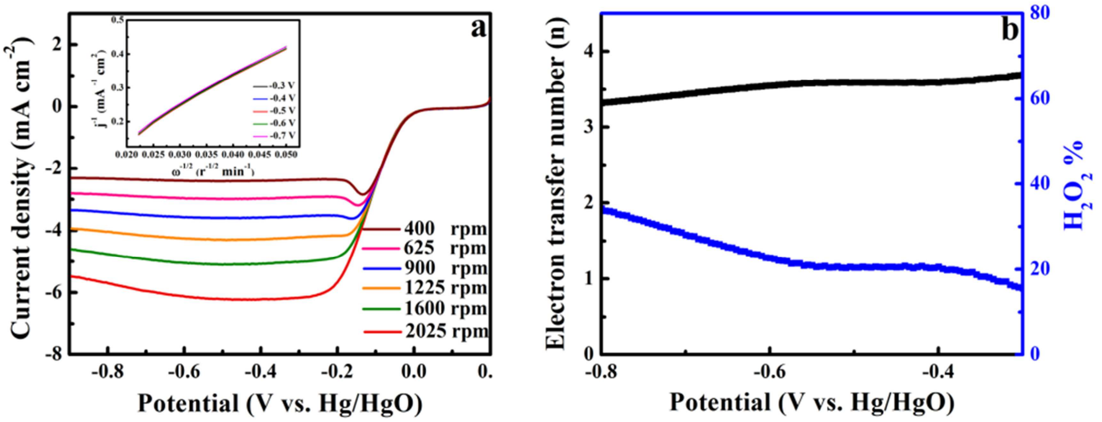

Fig. 7. (a) LSV curves of N-PC-4 at different rotation speeds from 400 rpm to 2025 rpm with a scan rate of 5 mV s^{-1} in O_2 statured 0.1 M KOH, the inset displays the K-L plots and electron transfer number of N-PC-4 sample. (b) The H_2O_2 yield and electron transfer number calculated from RRDE tests of N-PC-4 sample.

The LSV curves at various rotating speeds were tested to further describe ORR performance of N-PC-4 (Fig. 7a), and the corresponding K-L plots are given in the inset of Fig. 7a. The K-L plots are linear from - 0.30 to - 0.70 V, and the calculated number of transferred electrons (n) is 3.3. To further investigate the ORR progress of N-PC-4, RRDE measurement was undertaken at the potentials between -0.80 and -0.30 V. Using the formulas (3) and (4), the calculated electron transfer number is 3.31 to 3.68, and the H_2O_2 yield is within 34 % (Fig. 7b). This finding suggests that the optimized N-PC-4 is beneficial to the ORR process through an apparent/indirect four-electron pathway [28].

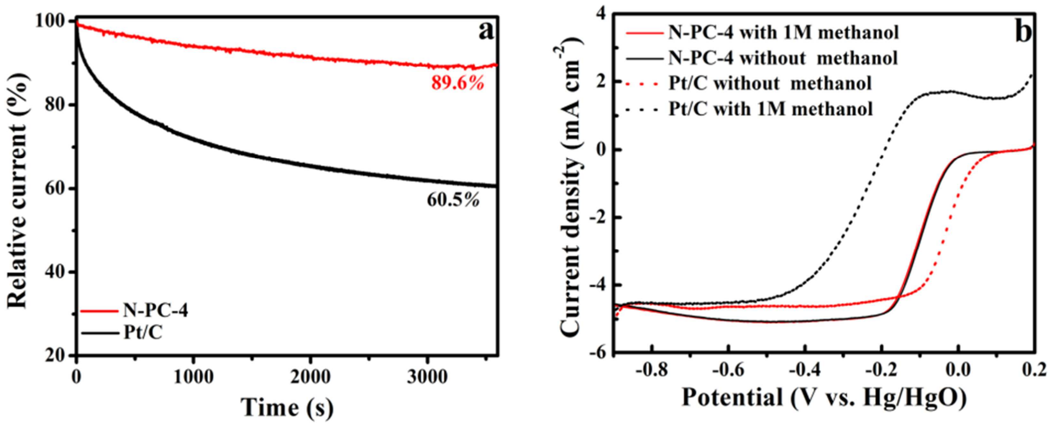

Fig. 8. (a) Chronoamperometric curves of N-PC-4 and Pt/C in O_2 saturated 0.1 M KOH solution at 0.30 V with the rotation speed of 1600 rpm. (b) Chronoamperometric responses of N-PC-4 and Pt/C in O_2 saturated in 0.1 M KOH solution after the addition of methanol.

The catalyst stability is a valuable parameter for the overall performance of a catalyst. The durability of N-PC-4 and Pt/C was tested by the CA and the results are shown in Fig. 8a. After 1 hour of continuous operation, the ORR current density retention is up to 89.6 % for N-PC-4, much better compared to Pt/C catalyst (60.5 %), indicating the superior ORR catalytic stability of the synthetic N-PC-4 catalyst. As methanol tolerance is very important for the actual application of ORR catalysts in fuel cells, the LSV responses for ORR before and after the addition of methanol were investigated on both N-PC-4 and Pt/C. As shown in Fig. 8b, a sharp CH_3OH oxidation peak is observed in LSV profile of Pt/C after 1 M methanol is added, accompanied with the negative shift of peak positions by more than 250 mV compared with the result of Pt/C in 0.1 M KOH without methanol. On the other hand, LSV profiles of N-PC-4 remain unchanged before and after the addition of CH_3OH, indicating the excellent methanol resistance of N-PC-4.

4. Conclusions

In this work, N-doped carbon nanosheets with hierarchical pore structure were facilely fabricated from soybean residue by solid-phase grinding combined with pyrolysis. g-C_3N_4 was used as both a sacrificial template and a nitrogen source to dope nitrogen and generate a plentiful mesopore structure. The optimized sample N-PC-4 shows favorable ORR catalytic activity, superior durability, and exceptional CH_3OH tolerance for ORR in alkaline electrolyte. This could be ascribed to the appropriate defect structure & level, high BET SA and pore volume, and abundance of N-containing active sites in N-PC-4 that benefiting to the ORR. This work supplies a very convenient and energy-saving strategy to fabricate efficient and economical ORR catalysts based on biomass waste.

Acknowledgement

This study was supported by the National Natural Science Foundation of China (21862021).

References:

[1] G. An, E. Lee, H. Ahn, Well-dispersed iron nanoparticles exposed within nitrogen-doped mesoporous carbon nanofibers by hydrogen-activation for oxygen-reduction reaction, J. Alloys Compd. 682 (2016) 746-752. https://doi.org/10.1016/j.jallcom.2016.05.033.

[2] M. Li, Y. Xiong, X. Liu, C. Han, Y. Zhang, X. Bo, L. Guo, Iron and nitrogen co-doped carbon nanotube@hollow carbon fibers derived from plant biomass as efficient catalysts for the oxygen reduction reaction, J. Mater. Chem. A 3 (2015) 9658-9667. https://doi.org/10.1039/C5TA00958H.

[3] J. Ma, D. Xiao, C. Chen, Q. Luo, Y. Yu, J. Zhou, X. Zuo, Uric acid-derived Fe3C-containing mesoporous Fe/N/C composite with high activity for oxygen

reduction reaction in alkaline medium, J. Power Sources 378 (2018) 491-498. https://doi.org/10.1016/j.jpowsour.2017.11.091.

[4] M. Wang, W. Yang, H. Wang, C. Chen, Z. Zhou, S. Sun, Pyrolyzed Fe–N–C composite as an efficient non-precious metal catalyst for oxygen reduction reaction in acidic medium, ACS Catalysis 4 (2014) 3928-3936. https://doi.org/10.1021/cs500673k.

[5] Q. Li, D. Xu, J. Guo, X. Ou, F. Yan, Protonated g-C_3N_4@polypyrrole derived N-doped porous carbon for supercapacitors and oxygen electrocatalysis, Carbon 124 (2017) 599-610. https://doi.org/10.1016/j.carbon.2017.09.029.

[6] C. Liu, J. Wang, J. Li, R. Luo, X. Sun, J. Shen, W. Han, L. Wang, Fe/N decorated mulberry-like hollow mesoporous carbon fibers as efficient electrocatalysts for oxygen reduction reaction, Carbon 114 (2017) 706-716. https://doi.org/10.1016/j.carbon.2016.12.083.

[7] S. Fu, C. Zhu, D. Su, J. Song, S. Yao, S. Feng, M. Engelhard, D. Du, Y. Lin, Porous carbon-hosted atomically dispersed iron-nitrogen moiety as enhanced electrocatalysts for oxygen reduction reaction in a wide range of pH, Small 14 (2018) 1703118. https://doi.org/10.1002/smll.201703118.

[8] J. Li, Y. Zhang, X. Zhang, J. Han, Y. Wang, L. Gu, Z. Zhang, X. Wang, J. Jian, P. Xu, B. Song, Direct transformation from graphitic C_3N_4 to nitrogen-doped graphene: An efficient metal-free electrocatalyst for oxygen reduction reaction, Acs Appl. Mater. Interfaces 7 (2015) 19626-19634. https://doi.org/10.1021/acsami. 5b03845.

[9] N. Daems, X. Sheng, I. Vankelecom, P. Pescarmona, Metal-free doped carbon materials as electrocatalysts for the oxygen reduction reaction, J. Mater. Chem. A 2 (2014) 4085-4110. https://doi.org/10.1039/C3TA14043A.

[10] B. Zhang, C. Wang, D. Liu, Y. Liu, X. Yu, L. Wang, Boosting ORR electrocatalytic performance of metal-free mesoporous biomass carbon by synergism of huge specific surface area and ultrahigh pyridinic nitrogen doping, ACS Sustainable Chem. Eng. 6 (2018) 13807-13812. https://doi.org/10.1021/acssuschemeng. 8b01876.

[11] C. Kim, C. Zhu, Y. Aoki, H. Habazaki, Exothermically efficient exfoliation of biomass cellulose to value-added N‑doped hierarchical porous carbon for oxygen reduction electrocatalyst, Ind. Eng. Chem. Res. 58 (2019) 3047-3059. https://doi.org/10.1021/acs.iecr.8b06410.

[12] Y. Liu, K. Sun, X. Cui, B. Li, J. Jiang, Defect-rich, graphenelike carbon sheets derived from biomass as efficient electrocatalysts for rechargeable Zinc−Air batteries, ACS Sustainable Chem. Eng. 8 (2020) 2981-2989. https://doi.org/10.1021/acssuschemeng.9b07621.

[13] Q. Li, T. He, Y. Zhang, H. Wu, J. Liu, Y. Qi, Y. Lei, H. Chen, Z. Sun, C. Peng, L. Yi, Y. Zhang, Biomass waste-derived 3D metal-free porous carbon as a bifunctional electrocatalyst for rechargeable Zinc−Air batteries, ACS Sustainable Chem. Eng. 7 (2019) 17039-17046. https://doi.org/10.1021/acssuschemeng.9b02964.

[14] X. Liu, Y. Zhou, W. Zhou, L. Li, S. Huang, S. Chen, Biomass-derived nitrogen self-doped porous carbon as effective metal-free catalysts for oxygen reduction reaction, Nanoscale 7 (2015) 6136-6142. https://doi.org/10.1039/C5NR00013K.

[15] T. Kumaresan, S. Gunasekaran, S. Elumalai, S. Masilamani, K. Raman, B. Rengarajan, R. Subashchandrabose, Promising nature-based nitrogen-doped porous carbon nanomaterial derived from borassus flabellifer male inflorescence as superior metal-free electrocatalyst for oxygen reduction reaction, Int. J. Hydrogen Energy 44 (2019) 25918-25929. https://doi.org/10.1016/j.ijhydene.2019.08.044.

[16] D. Shan, J. Yang, W. Liu, J. Yan, Z. Fan, Biomass-derived three-dimensional honeycomblike hierarchical structured carbon for ultrahigh energy density asymmetric supercapacitors, J. Mater. Chem. A 4 (2016) 13589-13602. https://doi.org/10.1039/C6TA05406D.

[17] P. Zhang, F. Sun, Z. Xiang, Z. Shen, J. Yun, D. Cao, ZIF-derived in situ nitrogen-doped porous carbons as efficient metal-free electrocatalysts for oxygen reduction reaction, Energy Environ. Sci. 7 (2014) 442-450. https://doi.org/10.1039/C3EE42799D.

[18] Z. Xu, J. Ma, M. Shi, Y. Xie, C. Feng, Biomass based iron and nitrogen co-doped 3D porous carbon as an efficient oxygen reduction catalyst, J. Colloid Interface Sci. 523 (2018) 144-150. https://doi.org/10.1016/j.jcis.2018.03.092.

[19] H. Yu, L. Shang, T. Bian, R. Shi, G. Waterhouse, Y. Zhao, C. Zhou, L.Wu, C. Tung, T. Zhang, Nitrogen-doped porous carbon nanosheets templated from g-C_3N_4 as metal-free electrocatalysts for efficient oxygen reduction reaction, Adv. Mater. 28 (2016) 5080-5086. https://doi.org/10.1002/adma.201600398.

[20] X. Wu, S. Li, B. Wang, J. Liu, M. Yu, From biomass chitin to mesoporous nanosheets assembled loofa sponge-like N-doped carbon/g-C_3N_4 3D network architectures as ultralow-cost bifunctional oxygen catalysts, Micro. Meso. Mater. 240 (2017) 216-226. https://doi.org/10.1016/j.micromeso.2016.11.022.

[21] S. Wang, G. Wang, T. Wu, Y. Zhang, F. Zhan, Y. Wang, J. Wang, Y. Fu, J. Qiu, BCN nanosheets templated by g-C_3N_4 for high performance capacitive deionization, J. Mater. Chem. A 6 (2018) 14644-14650. https://doi.org/10.1039/C8TA04058C.

[22] M.H. Shi, J.H. Ma, Z.Z. Yao, Z.W. Li, H.Y. Mi, Y.H. Xie, Iron and nitrogen co-doped porous carbon derived from soybean dregs with enhanced catalytic performance for oxygen reduction, J. Electroana. Chem. 839 (2019) 141-148. https://doi.org/10.1016/j.jelechem.2019.03.020.

[23] S. Wang, Z. Cui, J. Qin, M. Cao, Thermally removable in-situ formed ZnO template for synthesis of hierarchically porous N-doped carbon nanofibers for enhanced electrocatalysis, Nano Research 9 (2016) 2270-2283. https://doi.org/10.1007/ s12274-016-1114-x.

[24] Q. Yang, Z. Xiao, D. Kong, T. Zhang, X. Duan, S. Zhou, Y. Niu, Y. Shen, H. Sun, S. Wang, L. Zhi, New insight to the role of edges and heteroatoms in nanocarbons for oxygen reduction reaction, Nano energy. 66 (2019) 104096. https://doi.org/10.1016/ j.nanoen.2019.104096.

[25] J. Zhu, Y. Huang, W. Mei, C. Zhao, C. Zhang, J. Zhang, I. Amiinu, S. Mu, Effects of intrinsic pentagon defects on electrochemical reactivity of carbon nanomaterials.

Angew. Chem. Int. Ed. 58 (2019) 3859-3864. https://doi.org/10.1002/anie. 201813805.

[26] K.B. Wang, X.B. Shi, A.M. Lu, X.Y. Ma, Z.Y. Zhang, Y.A. Lu, H.J. Wang, High nitrogen-doped carbon/Mn_3O_4 hybrids synthesized from nitrogen-rich coordination polymer particles as supercapacitor electrodes. Dalton Trans. 44 (2015) 151–157. https://doi.org/10.1039/c4dt02456g.

[27] K.B. Wang, H.J. Wang, R. Bi, Y. Chu, Z.K. Wang, H. Wu, H. Pang, Controllable synthesis and electrochemical capacitor performance of MOF-derived MnO_x/N-doped carbon/MnO_2 composites. Inorg. Chem. Front. (6) 2019 2873–2884. https://doi.org/10.1039/c9qi00596j.

[28] N. Uehara, A. Ishihara, T. Nagai, M. Matsumoto, H. Imai, Y. Kohno, K. Matsuzawa, S. Mitsushima, K. Ota, Kinetic study of oxygen reduction reaction on tantalum oxide-based electrocatalysts produced from oxy-tantalum phthalocyanines in acidic media, Electrochim. Acta 182 (2015) 789-794. https://doi.org/10.1016/j.electacta. 2015.09.161.

N doped porous carbon materials (N-PC) were prepared by a facile strategy using biomass waste soybean residue as carbon source.The optimized N-PC presents superior catalytic activity and stability in ORR.

Declaration of interests

The authors declare that they have no known competing financial interests or personal relationships that could have appeared to influence the work reported in this paper.